



HAL
open science

Acetone degradation by cosmic rays in the solar neighbourhood and in the Galactic Centre

Diana Andrade, Ana de Barros, Jingjie Ding, Hermann Rothard, Philippe Boduch, Enio da Silveira

► **To cite this version:**

Diana Andrade, Ana de Barros, Jingjie Ding, Hermann Rothard, Philippe Boduch, et al.. Acetone degradation by cosmic rays in the solar neighbourhood and in the Galactic Centre. *Monthly Notices of the Royal Astronomical Society*, 2014, 444 (4), pp.3792-3801. 10.1093/mnras/stu1519 . hal-02349191

HAL Id: hal-02349191

<https://normandie-univ.hal.science/hal-02349191>

Submitted on 28 Jan 2022

HAL is a multi-disciplinary open access archive for the deposit and dissemination of scientific research documents, whether they are published or not. The documents may come from teaching and research institutions in France or abroad, or from public or private research centers.

L'archive ouverte pluridisciplinaire **HAL**, est destinée au dépôt et à la diffusion de documents scientifiques de niveau recherche, publiés ou non, émanant des établissements d'enseignement et de recherche français ou étrangers, des laboratoires publics ou privés.



Distributed under a Creative Commons Attribution 4.0 International License

Acetone degradation by cosmic rays in the solar neighbourhood and in the Galactic Centre

Diana P. P. Andrade,^{1,2★} Ana L. F. de Barros,³ Jingjie Ding,¹ Hermann Rothard,¹ Philippe Boduch¹ and Enio F. da Silveira⁴

¹Centre de Recherche sur les Ions, les Matériaux et la Photonique (CEA/CNRS/ ENSICAEN/Université de Caen-Basse Normandie), CIMAP-CIRIL-Ganil, Boulevard Henri Becquerel, BP 5133, F-14070 Caen Cedex 05, France

²Institute of Research and Development, Universidade do Vale do Paraíba, Av. Shishima Hifumi, 2911-Urbanova, São José do Campos, SP, Brazil

³Departamento de Física, Centro Federal de Educação Tecnológica Celso Suckow da Fonseca, Av. Maracanã 229, 20271-110 Rio de Janeiro, RJ, Brazil

⁴Departamento de Física, Pontifícia Universidade Católica do Rio de Janeiro, Rua Marquês de São Vicente 225, 22451-900 Rio de Janeiro, RJ, Brazil

Accepted 2014 July 25. Received 2014 July 25; in original form 2014 April 19

ABSTRACT

Acetone (CH_3COCH_3) was the first molecule with 10 atoms found in the interstellar medium. This molecule was found towards the hot molecular core Sagittarius B2 (N–LHM) and in the Orion–KL star-forming region towards the hot core. Laboratory data, such as the formation and destruction cross-sections and the half-life of the molecules, combined with theoretical calculations and astronomical observations, can help us to elucidate the processes that occur in the astronomical sources. In this work, we study the radiolysis of acetone ice by 40-MeV $^{58}\text{Ni}^{11+}$ ions at 16 K. Pure acetone ice was bombarded with nickel ions, which are cosmic ray constituents that are highly efficient at inducing chemical reaction in ices, in order to provide experimental data for a model describing interaction with similar heavy constituents of cosmic rays (with $z \geq 10$). The dissociation rate of pure acetone and its half-life in the interstellar medium in close proximity to the solar system and the Galactic Centre due to the main ions (H, He, C, Mg, O, Si, Fe, Ni) are predicted from recorded spectra and the current analysis. The formation of new molecular species by cosmic rays is discussed and the atom budget is analysed. The formation cross-section of species, as well as the penetration depth of some light and heavy ions, are also calculated. We present a discussion on the energy lost and the penetration depth of acetone ice.

Key words: astrochemistry – molecular data – methods: laboratory: molecular – cosmic rays – ISM: molecules.

1 INTRODUCTION

Acetone (CH_3COCH_3) has a central C = O structure, a strong bond present in several important molecules of astrophysical and biological interest. It was the first molecule with 10 atoms found in the interstellar medium (ISM), seen by Combes et al. (1987) and confirmed by Snyder et al. (2002) towards the hot molecular core Sagittarius (Sgr) B2 (N–LHM). Later, Friedel et al. (2005) have found acetone in the Orion–KL star-forming region towards the hot core. In addition, acetone was detected in the Murchison meteorite sample. According to Peng et al. (2013), acetone is an excellent tool for testing different chemical models of complex molecules productions (on the surface of grains and in the gas phase by cosmic ray induced ion-molecule chemistry, or both).

The formation of acetone in space is not yet well understood. Bennett et al. (2007) calculated the vibrational frequencies and band strengths for various species expected to be formed from pure ices of amorphous methanol, irradiated at 11 K by 5-keV electrons. This process of electronic energy transfer is similar to that occurring in interstellar ices, in comets and in icy Solar system bodies when irradiated by MeV ions and by secondary electrons produced in this interaction. According to Bennett et al. (2007), acetone is one of the species formed from the radiolysis of methanol. In some space environments, such as protostars W33A and RAFGL 7009, methanol is the most abundant solid-state substance after H_2O (Dartois et al. 1999; Pontoppidan et al. 2003a; Boogert et al. 2008). Ruiterkamp et al. (2005) found the 1072- and 1692- cm^{-1} bands after proton and ultraviolet (UV) irradiation of solid benzene and carbon monoxide mixture (1:20), but they could not attribute the new bands to any molecular species. Because acetone has a band at 1072 cm^{-1} and another at 1697 cm^{-1} , their results suggest the formation of acetone in an irradiated mixture of benzene and water.

★ E-mail: dianaufj@gmail.com

Ehrenfreund & Charnley (2000) have shown that grain mantle chemistry is required to explain the acetone formation in ISM gas. Therefore, the study of the interaction of the ionizing radiation with the acetone in the grain mantle should be important to understand how its fragmentation occurs in the solid state and how it leads to the synthesis of a more complex molecule. At a first stage, only pure acetone is studied. Recently, Almeida et al. (2014) studied the photostability of acetone ice using the white beam of synchrotron radiation (6–1200 eV). Ice degradation was monitored by near edge X-ray absorption fine structure (NEXAFS) spectroscopy around the O1s threshold. From this study, the photodissociation cross-section value of $1.2 \times 10^{-17} \text{ cm}^2$ was determined, allowing them to estimate the acetone half-life in astrophysical environments such as T Tauri stars, where soft X-rays play an important role in inducing chemical processes in grains.

Laboratory data, particularly the formation and destruction cross-sections and molecular half-lives, combined with theoretical calculations and astronomical observations are very helpful to elucidate the physico-chemical processes that occur in astronomical sources. Godard et al. (2011), de Barros et al. (2011a), de Barros et al. (2014) and Andrade et al. (2013) have suggested that the destruction cross-section (σ_d) relative to heavy ion irradiation follows a power law as a function of the electronic stopping power. To our knowledge, destruction cross-section values for acetone have not yet been measured and their dependence as a function of the stopping power is unknown. These destruction cross-sections allow us to predict the molecular half-life of acetone in the region of study for the considered projectiles.

To better understand the radiolysis of acetone and the subsequent synthesis of complex molecules, here we analyse the effects produced by the interaction of energetic ions with condensed (ice-phase) organic molecules. Pure CH_3COCH_3 ice was irradiated by high-energy ^{58}Ni ions, a cosmic ray constituent that should be highly efficient to induce chemical reaction in ices. The obtained data are expected to be representative of effects caused by all heavy constituents of cosmic rays (with $Z \geq 6$). The destruction cross-sections of pure acetone ice and its half-life in the ISM in the proximity of the Solar system and the Galactic Centre corresponding to different projectiles (H, He, C, Mg, O, Si, Fe, Ni) have been estimated from an interpolation of the current data with results from the literature. We present results concerning the production of new molecules from radiolysis of pure acetone ice, as well as a discussion on the penetration depth and energy loss by cosmic rays in this ice.

2 EXPERIMENTAL DETAILS

The experiments were performed at Grand Accélérateur National d'Ions Lourds (GANIL), Caen, France. Acetone vapour was condensed on a CsI substrate at 16 K and irradiated by 40-MeV $^{58}\text{Ni}^{11+}$ ($\sim 0.70 \text{ MeV u}^{-1}$) ions. The infrared (IR) analysis was performed *in situ* using a Fourier transform infrared (FTIR) spectrometer (Nicolet Magna 550) from 4000 to 600 cm^{-1} , with a resolution of 1 cm^{-1} . FTIR measurements were performed in the transmission mode. The chamber pressure during the experiments was below 2×10^{-8} mbar. Spectra at different fluences up to 1×10^{13} ion cm^{-2} were obtained for a sample of pure acetone and used to determine the cross-sections. Further details have been given elsewhere (Seperuelo Duarte et al. 2009; de Barros et al. 2011a, de Barros et al. 2011b).

The sample holding system could be rotated and placed in three different positions: gas deposition, FTIR measurement and perpendicular ion irradiation. The sample was purchased commercially

from Sigma-Aldrich with purity greater than 99.8 per cent, and further degassed through several freeze–pump–thaw cycles, before the vapour was admitted into the chamber. Using the density $\rho = 0.79 \text{ g cm}^{-3}$ (liquid) and the initial column density of the ice by band 1229.5 cm^{-1} ($N_0 = 2.24 \times 10^{18} \text{ molecule cm}^{-2}$), the ice thickness was determined to be 2.8 μm .

3 RESULTS

Fig. 1 shows the IR spectra of pure acetone before (solid line) and after (dotted line) irradiation. The band strengths (often referred to in this paper as the *A*-value, in cm molecule^{-1}) corresponding to other bands were calculated based on the 1229.5-cm^{-1} band (Bennett et al. 2007); see Table 1.

The acetone features have been identified following the work of Harris & Levin (1972). Acetone has 24 fundamental vibrations: six of these are associated with the skeletal framework and 18 vibration modes originate from hydrogen motions. In this work, only three of those skeletal modes arise and these are associated with C = O stretching and CC_2 symmetrical and antisymmetrical

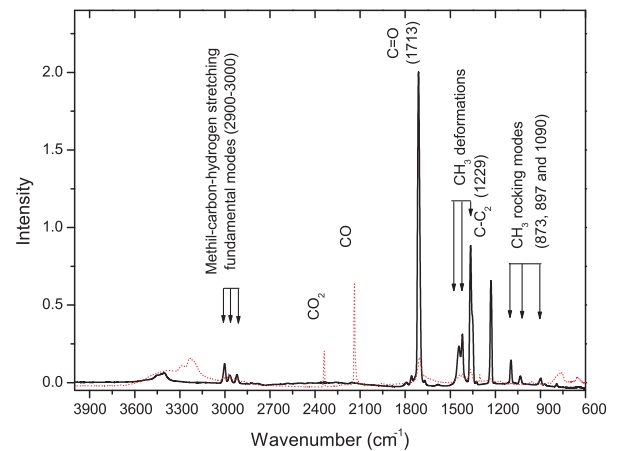


Figure 1. Experimental IR spectra of acetone ice at 13 K before (solid line) and after (dotted line) irradiation at fluences of 1×10^{13} ion cm^{-2} with 40-MeV $^{58}\text{Ni}^{11+}$ ions.

Table 1. Positions of the CH_3COCH_3 vibrational modes observed in this work, before irradiation, and those reported in the literature.

Position ^a (cm^{-1})	Position ^b (cm^{-1})	Assignments	<i>A</i> -values ^a ($\times 10^{-17}$ cm molecule^{-1})
791.1	796	CC_2 symmetrical stretch	^c
872.3	872	CH_3 rocking mode	0.020 ± 0.001
897.9	905	CH_3 rocking mode	0.050 ± 0.003
1070.0	1072	CH_3 rocking mode	0.017 ± 0.004
1096.0	1084	CH_3 rocking mode	0.21 ± 0.06
1229.5	1229	CC_2 antisymmetrical stretch	1.27^d
1351.8	1351	CH_3 symmetrical deformation	0.5 ± 0.03
1364.0	1366	CH_3 symmetrical deformation	1.3 ± 0.4
1419.1	1426	CH_3 symmetrical deformation	0.45 ± 0.06
1441.9	1444	CH_3 symmetrical deformation	0.76 ± 0.06
1711.0	1697	C = O stretching	5.2 ± 1.0
1758.2	1763	–	0.03 ± 0.002
2919.7	2920	CH_3 asymmetrical stretch	0.1 ± 0.03
2967.9	2972	CH_3 asymmetrical stretch	0.12 ± 0.03
3001.8	3004	CH_3 asymmetrical stretch	0.24 ± 0.03

Note: ^aThis work. ^bHarris & Levin (1972). ^cPeak area not reliable for this band. ^dBennett et al. (2007).

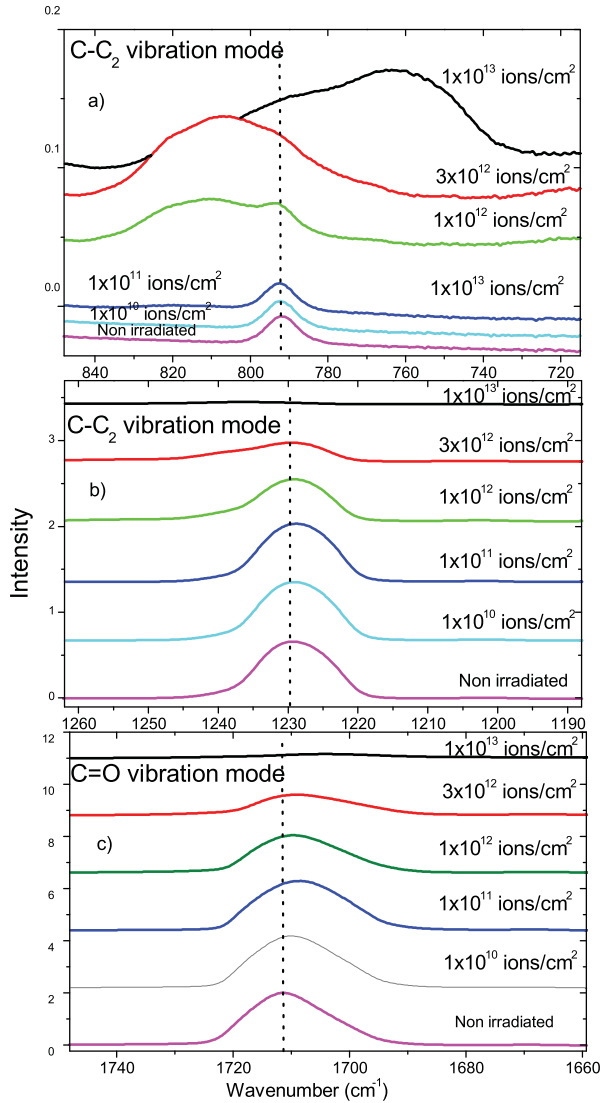


Figure 2. Zoom of the IR spectrum in wavenumbers near (a) 791.1 cm^{-1} , (b) 1229.5 cm^{-1} and (c) 1711.0 cm^{-1} . Both (a) and (b) are due to $\text{C}-\text{C}_2$ vibration modes, and (c) is due to the $\text{C}=\text{O}$ vibration mode.

stretching. The other three occur at smaller wavenumbers, in a range not visible by the spectrometry used. There are six methyl carbon–hydrogen stretching fundamental modes predicted to occur between 2900 and 3000 cm^{-1} . Because of the band splitting that arises from the in-phase and out-of-phase combinations of symmetrical and asymmetrical motions of the two methyl groups, the assignments of these modes are unclear. In the present work, only three of those bands are observed. Evolutions of selected acetone bands on fluence are presented in Figs 2 and 3.

3.1 Skeletal bands

Out of three bands of the acetone skeletal, two are related to the $\text{C}-\text{C}_2$ vibration mode and the third concerns the $\text{C}=\text{O}$ vibration mode. Figs 2(a) and (b) show a zoom of the IR spectrum at 791.1 and 1229.5 cm^{-1} due to $\text{C}-\text{C}_2$ vibration modes. The band at 791.1 cm^{-1} shifts as the fluence increases. In this work, the band at 1229.5 cm^{-1} is used as a reference to determine the destruction cross-section and to predict the acetone half-life in the astrophysical environments,

because this band appears as a single and isolated peak. The A -value for this band ($1.27 \times 10^{-17} \text{ cm molecule}^{-1}$) was proposed by Bennett et al. (2007) and was used to find the A -values of other acetone ice-band molecular species. In addition, as can be seen in Fig. 4, the small dispersion of the column density curves corresponding to eight bands indicates that the half-life dispersion is also small, making the choice of the reference band irrelevant. Harrison, Allen & Bernath (2011) found approximately the same A -value for this band, $1.12 \times 10^{-17} \text{ cm molecule}^{-1}$ for non-irradiated ices.

Fig. 2(c) shows the $\text{C}=\text{O}$ band at 1711.0 cm^{-1} . This band is shifted as the fluence increases and there are two other vibration modes in its range, according to Harris & Levin (1972). The A -values are presented in Table 1.

3.2 Destruction cross-sections of precursors

The destruction cross-section can be obtained from the dependence of the molecular column density on beam fluence. Because the loss energy ΔE of the projectile during the experiment is negligible compared with the projectile initial energy E_0 ($\Delta E \ll E_0$), the destruction cross-section can be considered constant along the projectile track in the sample.

The determination of the destruction cross-section is based on the hypothesis that the column density $N(F)$ is proportional to the area of the band in the spectrum, for any beam fluence F . The $N(F)$ rate is given by (Seperuelo Duarte et al. 2010; Mejía et al. 2013)

$$\frac{dN_i}{dF} = \sum_{j \neq i} \sigma_{f,ij} N_j + L_i - \sigma_{d,i} N_i - Y_i, \quad (1)$$

where N_i is the column density of the molecular species i as a function of the beam fluence F , $\sigma_{f,i}$ and $\sigma_{d,i}$ are its formation and its destruction cross-sections, respectively, and L_i and Y_i are the partial layering and sputtering yields. For the current measurement, the gas entrance valve was effectively close and all the gas-phase acetone inside the chamber had a negligible partial pressure (the gaseous acetone was already condensed or pumped out). Therefore, the acetone layering is absent ($L_1 = 0$). In addition, a very thin layer of residual water condensed over the acetone ice surface and acetone molecules cannot be ejected from the target by the ion beam impact. For this reason, the acetone sputtering was considered negligible during the irradiation ($Y_1 = 0$).

The column density of water is seen by the IR spectrometer only at fluences higher than $1 \times 10^{12} \text{ ion cm}^{-2}$. The major effect produced by the H_2O layering is to inhibit progressively the acetone sputtering up to its complete extinction. Thus, a single exponential function should describe correctly the fluence dependence.

At the beginning of the experiments, some peak areas in the spectra decrease with the fluence, while others increase. This occurs because of the structural changes in the ices during the irradiation. The fact that the band area seems to increase very fast at the beginning of irradiation is attributed to ice compaction; during this process, the A -value of the IR absorption changes. Figs 3(a)–(e) show zooms of spectra relative to some acetone bands at different fluences. Fig. 3(f) shows an example of the Gaussian fitting used to determine the area of the bands.

To determine the destruction cross-sections of the skeletal bands, whose data are presented in Fig. 5(a), and the ones for methyl vibration modes shown in Figs 5(b), (c) and (d), the column density evolution on fluence for each precursor species i should be approximately described by the differential equation system given by equation (1). The obtained value for the destruction cross-section

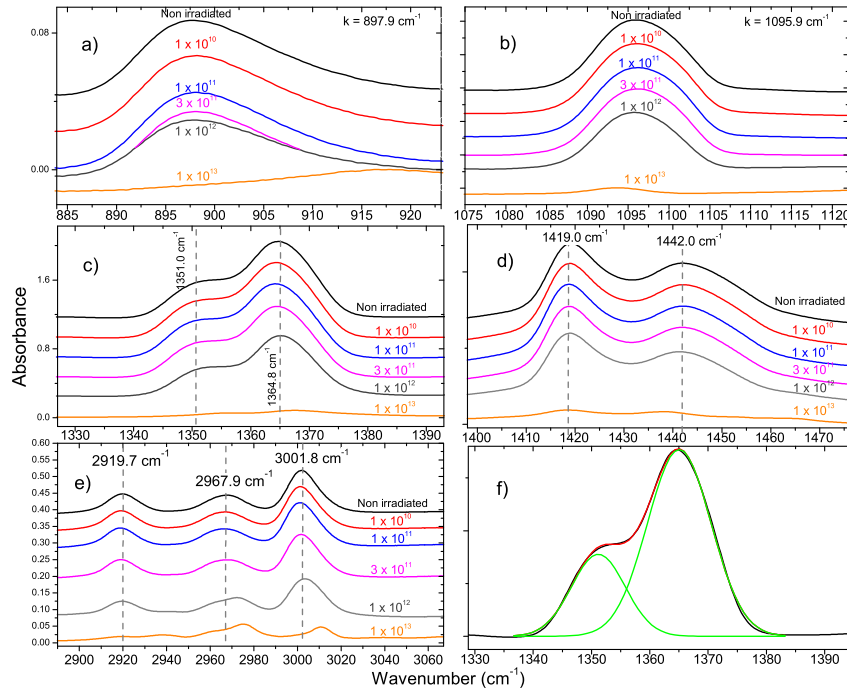


Figure 3. (a)–(e) Particular acetone bands at different fluences. (f) An example of the Gaussian fitting used to determine the total band absorbance (peak areas).

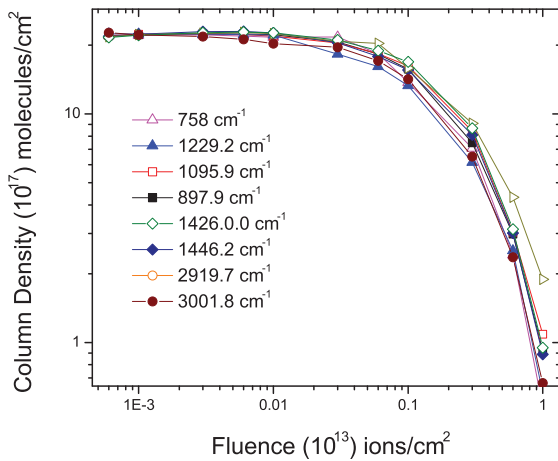


Figure 4. Evolution of the acetone molecular column density as a function of the fluence, considering the different vibration modes observed in the IR spectra and the A -values proposed in this work.

(σ_d) for acetone was $3.6 \times 10^{-13} \text{ cm}^2$, using, as a reference, the band CC_2 (1229.5 cm^{-1}) (see Table 2). This value was used to calculate the half-life of pure acetone in the ISM (details in Section 5.2).

3.3 Daughter species: CH_4 , CO , H_2CO , CO_2 , C_2H_4 , C_2H_6

The most abundant species formed by the Ni ion bombardment of pure acetone are CH_4 , CO , H_2CO , CO_2 , C_2H_4 and C_2H_6 . Fig. 6 shows the column density evolution for these species as a function of the fluence and Fig. 7 shows the fittings of acetone column density variation using equations (3)–(5). Table 3 displays the A -values for the molecular species produced under irradiation of the CH_3COCH_3 ice used in this work.

(i) The CH_4 molecules are identified by their relatively isolated ν_4 band at 1302 cm^{-1} (D’Hendecourt et al. 1986). The A -value used for this band is $5.1 \times 10^{-18} \text{ cm molecule}^{-1}$ (Gerakines, Schutte & Ehrenfreund 1996; de Barros et al. 2011b); its column density determined after irradiation is $N = 2.24 \times 10^{18} \text{ molecule cm}^{-2}$.

(ii) The CO absorption feature has been observed astronomically by three multiple components: two relatively narrow features around 2139.7 cm^{-1} (Gerakines et al. 1995) and 2143.7 cm^{-1} (Boogert, Hogerheijde & Blanke 2002; van Broekhuizen et al. 2006) and a broader component around 2136.5 cm^{-1} (Tielens et al. 1991; Ehrenfreund et al. 1997; Boogert et al. 2002; Pontoppidan et al. 2003b). In the present experiment, only the 2136-cm^{-1} feature was observed. This particular feature does not correspond to any other species and the identification is thus clear. The column density of carbon monoxide was traced through the CO stretching at 2136 cm^{-1} using the A -value equal to $1.1 \times 10^{-17} \text{ cm molecule}^{-1}$ (Gerakines et al. 1995). The column density of carbon monoxide increases slightly with fluence reaching the column density of $N = 1.85 \times 10^{17} \text{ molecule cm}^{-2}$ after irradiation.

(iii) H_2CO has a strong band at 1165 cm^{-1} . This band is relatively isolated and has been used previously to constrain H_2CO production (Bennett et al. 2007). The column density after irradiation with the A -value of $4.28 \times 10^{-18} \text{ cm molecule}^{-1}$ (Bennett et al. 2007) is $N = 8.33 \times 10^{16} \text{ molecule cm}^{-2}$; its evolution can be seen in Figs 7(a) and (b).

(iv) CO_2 has a strong band at 2346 cm^{-1} (CO stretch), which is seen in all experiments at high fluence. This spectral region appears to be polluted with bands from unavoidable residual CO_2 contamination. The column density of carbon dioxide after irradiation, using an A -value of $7.6 \times 10^{-17} \text{ cm molecule}^{-1}$ (Gerakines et al. 1995), is $N = 3.96 \times 10^{16} \text{ molecule cm}^{-2}$ and is approximately equal to that of carbon monoxide.

(v) The column density of C_2H_4 was traced through the ν_7 assignment at 955 cm^{-1} using an A -value of $15 \times 10^{-18} \text{ cm molecule}^{-1}$

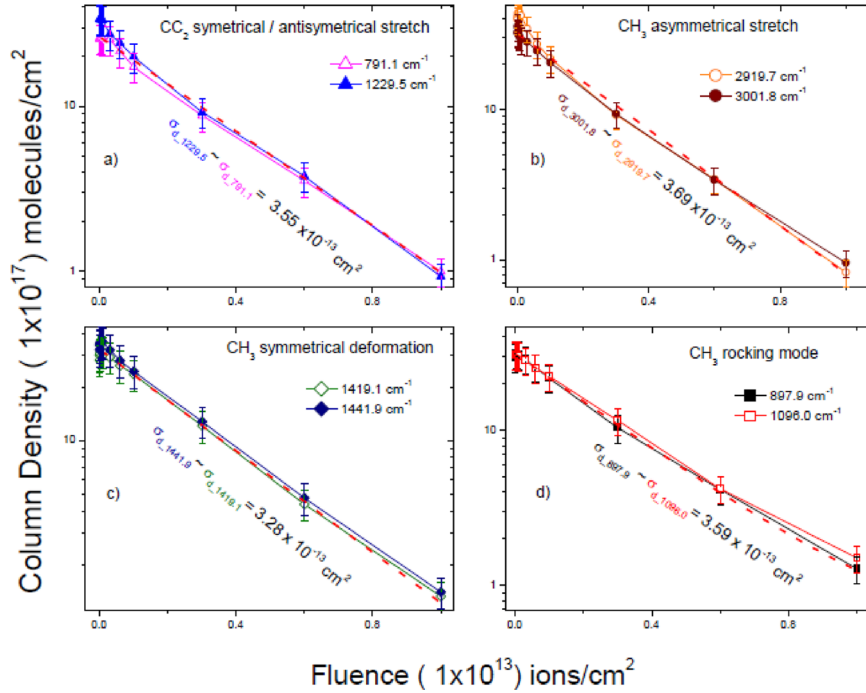


Figure 5. Acetone column density variation measured for different bands. Solid curves are guides for the eyes; dash lines are the prediction of Eq 1 for $Y1 = L1 = \text{Sigma}, f, 1 = 0$. The acetone destruction cross-section is determined independently through the analysis of four vibration modes.

Table 2. Destruction cross-section value, depending on the selected CH_3COCH_3 vibration mode.

Vibration mode	Destruction cross-section ($\times 10^{-13} \text{ cm}^2$)
CC_2 symmetrical and antisymmetrical stretch	3.6 ± 0.9
CH_3 symmetrical deformation	3.3 ± 0.8
CH_3 asymmetrical stretch	3.7 ± 0.7
CH_3 rocking mode	3.6 ± 0.9

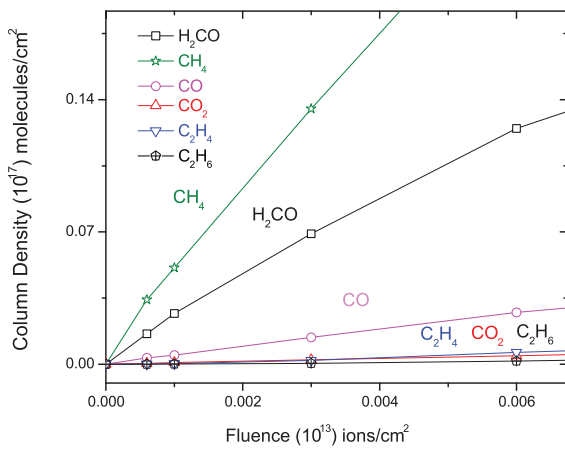


Figure 6. Zoom in the low fluence region showing the dependence of the column density behaviour of daughter species on fluence.

(Mejía et al. 2013). The column density after irradiation was found to be $N = 1.79 \times 10^{16} \text{ molecule cm}^{-2}$. This column density value does not evolve too much with the increase of the fluence.

(vi) C_2H_6 is observed at the 2881-cm^{-1} band. The A -value for C_2H_6 bands was adopted as $3.2 \times 10^{-17} \text{ cm molecule}^{-1}$ (de Barros et al. 2011b; Bennett et al. 2006). The column density after irradiation was found to be $N = 9.61 \times 10^{15} \text{ molecule cm}^{-2}$. The formation cross-sections of both bands C_2H_4 and C_2H_6 have similar behaviour with fluence, being proportional to the function F^2 .

3.4 Formation and destruction cross-sections of daughter species

Following the methodology used in previous work (Mejía et al. 2013), the formation and destruction cross-sections of daughter species were obtained by solving equation (1). The approximate solution is

$$N_i(F) = N_{1,0} \frac{\sigma_{f,i1}}{(\sigma_{d,1} - \sigma_{d,i})} [\exp(-\sigma_{d,i} F) - \exp(-\sigma_{d,1} F)], \quad (2)$$

where $\sigma_{f,i1}$ and $\sigma_{d,i}$ are the formation and destruction cross-sections of daughter species i and $\sigma_{d,1}$ is the total (summed over all the final states) destruction cross-section of the acetone.

Considering the low fluence region (the beginning of the irradiation), $\sigma_d F \ll 1$, this expression reduces to

$$N_i(F) \approx N_{1,0} \sigma_{f,i1} \left[F - \frac{1}{2} (\sigma_{d,1} + \sigma_{d,i}) F^2 \right], \quad (3)$$

which shows that $\sigma_{f,i1}$ is proportional to the $N(F)$ slope and the sum $\sigma_{d,1} + \sigma_{d,i}$ is responsible for levelling off the curve.

If n_k acetone molecules are necessary for the formation of species k , the formation cross-sections can be redefined as

$$\sigma_{d,1} = \sum_k n_k \sigma_{f,k} = \sum_k \sigma_{f,k}^*. \quad (4)$$

The branching ratio $\sigma_{f,k}^*/\sigma_{d,1}$ gives the probability of forming the daughter species k when acetone radiolysis occurs.

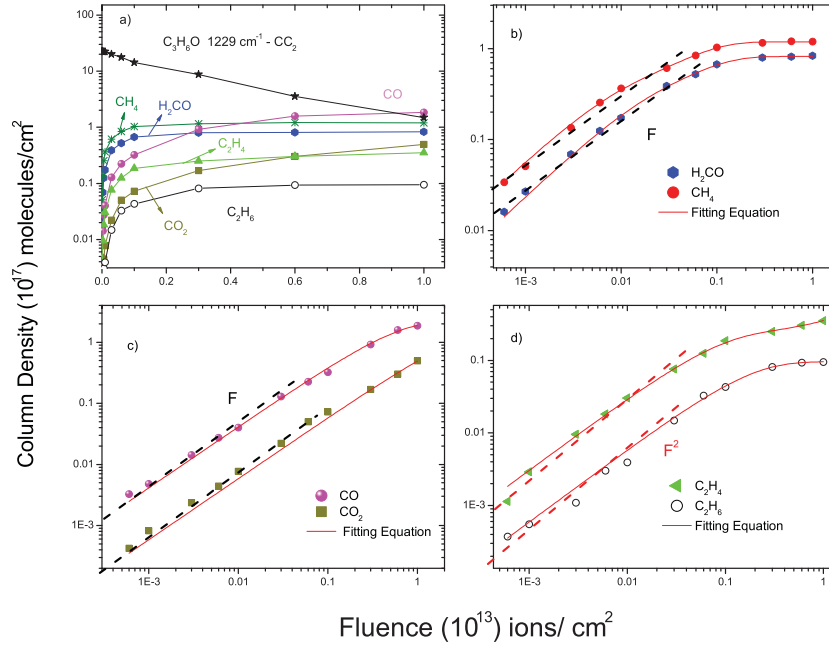


Figure 7. Evolution of the column densities of C_3H_6O and of the most abundant produced species corresponding to the nickel beam irradiation at temperatures of 16 K. The solid and dashed curves are predictions from equations (2) and (3) for daughter species. The extracted cross-sections are presented in Table 3. At low fluence, the C_2H_4 and C_2H_6 data increase linearly with F^2 , as predicted by equation (5).

Table 3. The final column density ($N_{k,f}$), A -value, formation (σ_f) and destruction (σ_d) cross-sections obtained by fitting the column density evolution of daughter species with equations (2) and (3) and the radiochemical yields G_f (formation) and G_d (destruction) with $S_e = 4.8 \times 10^2$ eV $cm^2/10^{15}$ atom.

Species	$N_{k,f} \times 10^{16}$ (molecule cm^{-2})	A -value (cm molecule $^{-1}$)	$\sigma_f \times 10^{-14}$ (cm^2)	$\sigma_d \times 10^{-14}$ (cm^2)	G_f (molec/100 eV)	G_d (molec/100 eV)
H_2CO	6.59	0.43 ^a	4.0 ± 0.2	1.4 ± 0.4	0.08	0.090
CH_4	3.72	11 ^{b,c}	6.6 ± 0.9	1.6 ± 0.5	0.13	0.330
CO	11.20	7.6 ^{c,d}	1.5 ± 0.5	0.16 ± 0.04	0.03	0.003
CO_2	7.26	3.2 ^e	2.6 ± 0.6^f	0.35 ± 0.01	0.05	0.007
C_2H_4	2.24	1.5 ^a	4.4 ± 0.8	1.2 ± 0.3	0.09	0.030
C_2H_6	5.62	0.51 ^{b,c}	0.59 ± 0.03	2.4 ± 0.6	0.01	0.050

Note: ^aBennett et al. (2007). ^bGerakines, Schutte & Ehrenfreund (1996). ^cde Barros et al. (2011b). ^dJamieson, Mebel & Kaiser (2006). ^eMejía et al. (2013). ^fCross-sections are multiplied by two, because these species need two precursor molecules.

The approximate solution for ‘granddaughter’ species is

$$N_k(F) \approx N_i(F) \frac{\sigma_{f,ki}}{2} F \approx N_{i,0} \frac{\sigma_{f,i} \sigma_{f,ki}}{2} F^2. \quad (5)$$

The fittings using equations (3)–(5) are presented in Fig. 7.

The current experimental data were fitted using a decaying exponential for acetone, equation (2) for CO , CO_2 , H_2CO and CH_4 data and equation (5) for C_2H_4 and C_2H_6 . Indeed, the data of Fig. 7(d) show that neither C_2H_4 nor C_2H_6 can be fitted by equations (2) or (3), because their column densities are proportional to F^2 . This means that they are not direct daughters of the acetone but, instead, they could be ‘granddaughter’ species; accordingly, they must be fitted by equation (5). The obtained formation cross-sections of the daughter species are displayed in Table 3.

4 ATOM BUDGET

At a given beam fluence, the balance between the number of atoms of each element existing in the sample, as constituents of precursor molecules, and the number of atoms of the same element constituent

of the observed daughter molecules is called the atom budget. If sputtering and layering are negligible and if the majority of daughter molecular species gives the FTIR signal, then the balance must be obtained independently for each atomic element. This condition comes simply from the fact that chemical reactions rearrange atoms and cannot change their identities. The relevance of this analysis is to verify if the relative A -values are consistent or, inversely, if the majority of the daughter species can be scanned by FTIR.

Figs 8(a) and (b) present the evolution of the atomic column densities as a function of the beam fluence for carbon and for hydrogen and oxygen, respectively. The partial values are determined for the most abundant daughter molecular species according to their stoichiometry.

According to this analysis, it is noted that, along the irradiation, about 20 per cent of carbon atoms originated from the destroyed acetone molecules reappear in the detected products. Similar observations are found for the hydrogen and oxygen atoms. These results reveal that most of the overall flux of rearranged atoms is not controlled for the current observations.

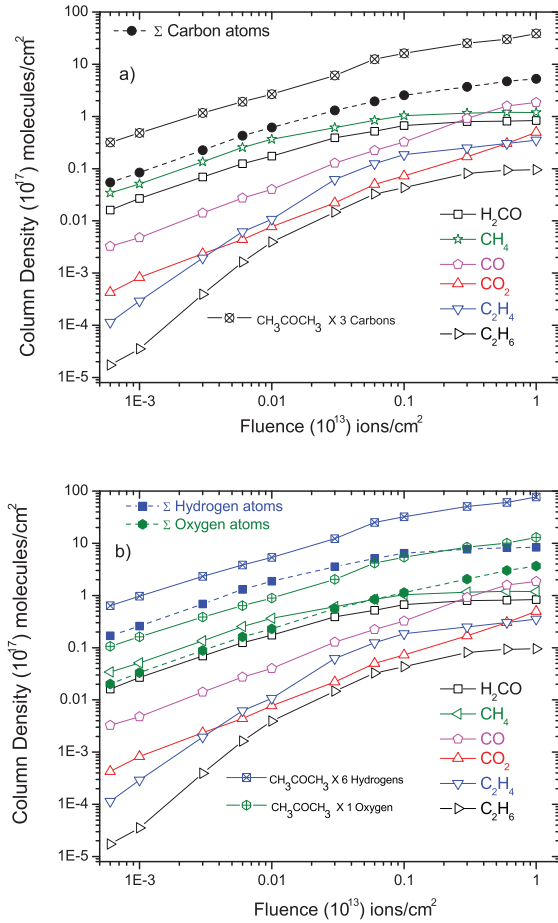


Figure 8. Atomic column densities of the bombarded ice as a function of the Ni beam fluence for (a) carbon atoms and (b) hydrogen and oxygen atoms. Open symbols are partial values corresponding to each daughter molecular species. Solid symbols refer to the sum of the partial values of formed molecules. These values are to be compared to the atomic column densities of the destroyed precursor molecules (open symbols with a \times or $+$ inside).

5 ASTROPHYSICAL IMPLICATIONS

5.1 Penetration depth and energy loss of cosmic ray particles

Surfaces in space are bombarded by light and heavy ions, which transfer part or all of their kinetic and potential energy to the molecules of solids. These impacts produce secondary electrons and photons, inducing further ionization, molecular destruction, desorption and chemical reactions. The penetration range, as well as the heating due to the ion impacts, depend on the initial energy of the incident ion and on the target material. According to Prasad & Tarafdar (1983), the cosmic rays seem to be mainly responsible for the chemical evolution of the molecular clouds, inducing desorption from the grains in the ISM. Furthermore, absorption and scattering by dust prevent UV photons from penetrating the inner and dense regions of these objects, because typical cosmic rays have an average penetration depth higher than UV photons. Fig. 9(a) shows the penetration depth of some light and heavy ions inside acetone ice, as predicted by the SRIM program (Ziegler, Ziegler & Biersack 2010), considering its density as $\rho = 0.79 \text{ g cm}^{-3}$. Fig. 9(b) shows the energy lost inside the ice by the incident ion per $0.1 \mu\text{m}$. From these figures, we note the following.

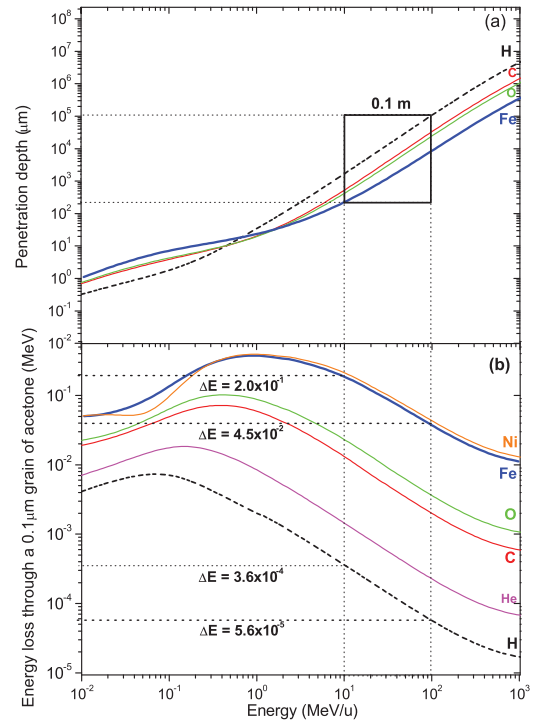


Figure 9. (a) The penetration depth of some light and heavy ions inside acetone ice (density $\rho = 0.79 \text{ g cm}^{-3}$), as predicted by the SRIM program, for different projectiles. (b) The energy lost by the incident ion per $0.1 \mu\text{m}$ of ice thickness.

(i) For velocities corresponding to $10^{-2} \leq E \text{ (MeV u}^{-1}\text{)} \leq 10^{-1}$, Fe and other heavy ions reach deeper layers than protons or He ions. Therefore, Fe ions are more efficient than hydrogen at inducing chemical reactions in the bulk. In this velocity range, the energy rate transferred by heavy ions is ~ 10 times higher than that of light ions, because they penetrate the ice.

(ii) For velocities close to the maximum cosmic ray flux in the ISM ($E/m = \sim 50\text{--}100 \text{ MeV u}^{-1}$), indicated by the horizontal side of the rectangle in Figs 9(a) and (b), Fe ions penetrate less than light ones, having a penetration depth about 10 times lower than hydrogen. Although heavy and light ions participate in inducing desorption, Fe and Ni ions transfer 10^3 times more energy than H and He ions when traversing $0.1 \mu\text{m}$ of ice. C and O ions have approximately the same penetration depths as each other, which are intermediary values between those of Fe and H.

5.2 Acetone molecular half-life in the ISM and in the Solar neighbourhood

Godard et al. (2011) have suggested that the destruction cross-section σ_d relative to heavy ion irradiation follows a power law as a function of the electronic stopping power S_e , and is $\sigma_d \propto S_e^{1.3}$ for the C–H destruction cross-section. De Barros et al. (2011a) and Andrade et al. (2013), based on experiments with irradiated methanol and formic acid ice, respectively, have found that the destruction cross-sections σ_d of those molecules due to heavy ion interaction also follow a power law as a function of the electronic stopping power. For the analysed precursor and daughter species, $\sigma_d = a S_e^n$, where $n = (1.5 \pm 0.3)$.

The SRIM code (Ziegler et al. 2010) was used to calculate the electronic stopping power S_e in acetone ice of the most abundant cosmic ray ions. To our knowledge, destruction cross-section values

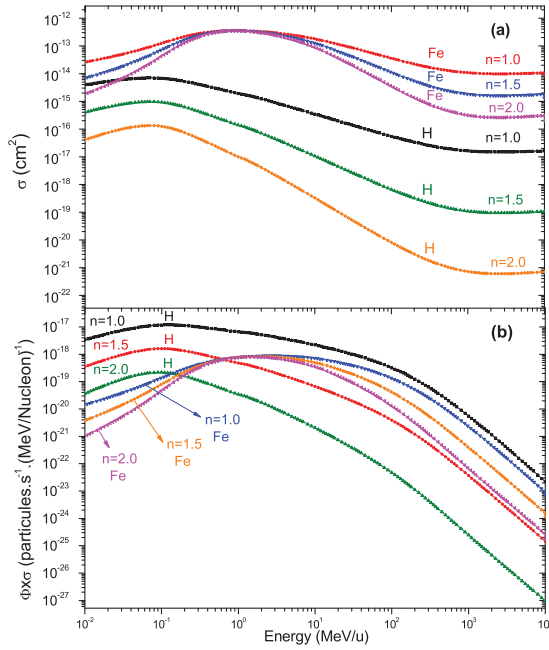


Figure 10. (a) Dependence on energy of the destruction cross-section for acetone for several n power values. (b) Dependence of dissociation rates on projectile energy. Calculations performed only for hydrogen and iron ions.

for acetone have not yet been measured and their dependence as a function of the stopping power is unknown. For this purpose, simulations have been performed with five values for n ($n = 1.0, 1.25, 1.5, 1.75$ and 2.0). The factor a was estimated using the S_e data for 40-MeV Ni ions in acetone ice and the destruction cross-section value obtained in this work for the ν_s ($C-C_2$) band, at 1229.5 cm^{-1} (Table 2). This destruction cross-section permits the prediction of the molecular half-life of acetone in the region of study for the considered projectiles.

Fig. 10(a) shows the predicted dependence on kinetic energy of the acetone destruction cross-section for six values of the power n , considering only hydrogen and iron projectiles. Although hydrogen is the most abundant cosmic ray constituent in the ISM, Fe/Ni ions have a much higher stopping power among the analysed projectiles. Consequently, the destruction cross-section due to Fe is higher than that due to H. The acetone dissociation rate (Fig. 10b), defined as the product ($\Phi_k \times \sigma_d$), is dominant for hydrogen at low velocities and for Fe, at high velocities. Fig. 11 shows the predicted dissociation rates for acetone due to the main cosmic rays constituents, considering the power $n = 1.5$. For other heavy ions such as Si, Mg and Ni, the dissociation rate increase is not so significant. As a consequence, Fe ions appear to be mainly responsible for the radiolysis of frozen acetone and other organic molecules in the ISM.

Table 4 shows the n -values considered in this work, the value of the parameter a due to each n -value and the half-lives for acetone. The quantity τ_{H+He} is the half-life due to the light ions H and He and τ_{Heavy} is the half-life considering the heavy ions C, O, Mg, Si, Fe and Ni. In this table, the label ISM corresponds to the total half-life considering the eight cosmic ray main constituents H, He, C, O, Mg, Si, Fe and Ni. If $n = 1.0$, hydrogen and helium ions determine the acetone half-life, while if $n \geq 1.25$, the acetone is mainly destroyed by heavier ions.

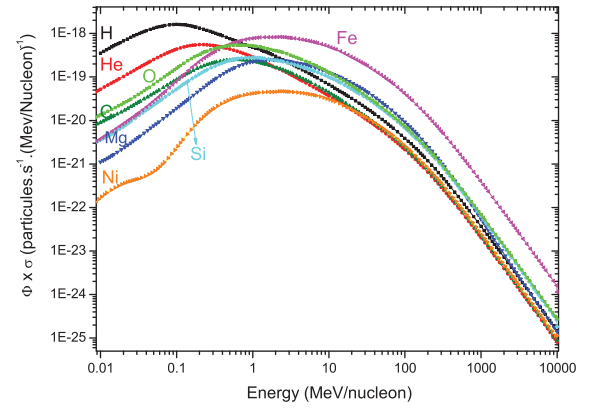


Figure 11. Predicted dissociation rates for acetone due the main cosmic ray constituents. The power $n = 1.5$ was considered.

Table 4. Molecular half-life of acetone in the ISM in the solar neighbourhood for different n -values in the equation $\sigma = aS_e^n$. In the third column, only the interaction with H and He projectiles is considered. τ_{Heavy} corresponds to C, O, Mg, Si, Fe and Ni projectiles. In the last column, the contributions of all eight projectile species are included in the calculation.

n	$a \times 10^{-18}$	τ_{H+He} (10 ³ Ma)	τ_{Heavy} (10 ³ Ma)	τ_{ISM} (10 ³ Ma)
1.00	738.00	0.11	0.15	0.06
1.25	156.00	0.68	0.29	0.20
1.50	33.00	3.55	0.67	0.57
1.75	6.97	15.50	0.79	0.79
2.00	1.47	58.10	1.15	1.13

5.3 Acetone molecular half-life in the Galactic Centre region

Using observations from the National Radio Astronomy Observatories (NRAO) 12-m telescope and the Berkeley–Illinois–Maryland Association (BIMA) array, Snyder et al. (2002) detected 13 new interstellar acetone emission features [CH_3COCH_3]. These assignments are based on the frequencies measured and calculated by Groner et al. (2002), and have also been confirmed by Combes et al. (1987) in their interstellar acetone identification. According to Snyder et al. (2002), the emission of acetone is concentrated in the vicinity of the hot molecular core Sgr B2 (N–LMH), and its beam-averaged column density is $N = 2.9 \times 10^{16} \text{ molecule cm}^{-2}$. In these regions, other organic molecules, such as methanol, have also been found. Using the Long Wavelength Spectrometer (LWS) instrument onboard the *Infrared Space Observatory (ISO)*, a strong emission of dust was observed through the entire molecular cloud. According to Goicoechea, Rodriguez-Fernandez & Cernicharo (2004), the fittings for this dust indicated two temperature components T_d : one cold ($T_d \sim 13\text{--}22 \text{ K}$) and another warmer ($T_d \sim 24\text{--}38 \text{ K}$). The gas kinetic temperature T_k in the direction of Sgr B2 is higher ($T_k \sim 200 \text{ K}$), according to the NH_3 line analysis made by Hüttemeister et al. (1995) and Ceccarelli et al. (2002). They suggested that shocks are a possible mechanism for gas heating. This has indeed been confirmed by observations of high-velocity components of HCO^+ , HNC and SiO towards Sgr B2 (Kuan & Snyder 1996; Martín-Pintado et al. 1997; Minh et al. 1998), suggesting the possibility of cloud–cloud collisions.

The X-ray luminosity in Sgr B2 is low ($L_x \sim 10^{35} \text{ erg s}^{-1}$), according to Murakami, Koyama & Maeda (2001). Considering

Table 5. Molecular half-life of acetone close to the Galactic Centre for different n -values in the equation $\sigma = aS_e^n$.

n	Cosmic rays		X-rays	
	$\tau_{\text{SgrB2(OH)}}$ (Ma)	$\tau_{\text{Sgr(A)}}$ (Ma)	d (pc)	τ_{SgrB2} (Ma)
1.00	6.4	2.1	1	1.1×10^{10}
1.25	20.4	6.8	10	1.1×10^{12}
1.50	56.5	18.8	50	2.8×10^{13}
1.75	79.0	26.3	70	5.4×10^{13}
2.00	112.5	37.5	100	1.1×10^{14}

that Sgr B2 is 1 pc distant from the X-ray source, a low incident X-ray flux in the gas ($F_x \sim 10^{-3} \text{ erg cm}^{-2} \text{ s}^{-1}$) is expected. However, this massive molecular cloud, which lies near the Galactic Centre, is almost certainly a region of enhanced cosmic rays. The cosmic ray ionization rate, ζ_{CR} , for the Sgr B2 region was estimated by van der Tak et al. (2006). Considering the observed $\text{H}_3\text{O}^+/\text{H}_2\text{O}^+$ ratio in the Sgr B2 envelope (OH), the cosmic ray ionization rate is $\zeta_{\text{CR}} \sim 4 \times 10^{16} \text{ s}^{-1}$, a value 10 times higher than the value found by van der Tak & van Dishoeck (2000) for the dense gas in the Solar neighbourhood, but three times lower than indicated by H_3^+ observations in the direction of Sgr A (Oka et al. 2005). This suggests that for dense molecular clouds, the cosmic ray flux can vary by one order of magnitude, resulting in different ionization rates, depending on their location in the Galaxy. Van der Tak & van Dishoeck (2000) have shown that the bulk of the ionization in dense star-forming regions is due to cosmic rays, with a rate of $\zeta_{\text{CR}} \sim 3 \times 10^{-17} \text{ s}^{-1}$, derived from HCO^+ and CO emission lines of the envelopes of young massive stars up to a few kpc from the Sun. The ionization rate of interstellar clouds is a key parameter for understanding the dynamics and chemistry of these environments (Caselli & Walmsley 2001).

In addition, the half-life for acetone in Sgr B2 and Sgr A due to X-ray photons can also be estimated using the data from Almeida et al. (2014), who have studied the photostability of acetone by exposing it to different irradiation doses with a white beam of synchrotron radiation (6–1200 eV). The degradation of the ice was monitored by NEXAFS spectroscopy around the O1s threshold. From this study, the photodestruction cross-section for acetone was determined to be $\sigma_D = 1.2 \times 10^{-17} \text{ cm}^2$. This result allows us to estimate the half-life for acetone ice in astrophysical environments where UV and soft X-rays play an important role in chemical processes.

Table 5 shows the half-life calculated for pure acetone in the direction of the Galactic Centre. The first column depicts the n -value used in the equation $\sigma_d = aS_e^n$. The second and third columns are the half-lives predicted for acetone in Sgr B2 (OH; in the envelope region) and in the vicinity of the hot molecular core Sgr B2 (M) due to cosmic ray impacts. The fourth and fifth columns concern the half-life in Sgr B2 due to X-rays at different distances d in parsec (pc) of the X-ray source. For X-ray irradiation, the half-lives are estimated using $\tau_{1/2} = \ln(2)/(\sigma_D \times \Phi)$, where σ_D is the destruction cross-section for acetone determined by Almeida et al. (2014) and Φ is the X-ray flux in the studied region. Table 5 presents the results for acetone at a distance of 1 pc from the X-ray source.

6 REMARKS AND CONCLUSIONS

In this work, we have studied the radiolysis of 16-K pure acetone ice by 40-MeV $^{58}\text{Ni}^{11+}$ ions. The data obtained for the interaction

nickel beam-ice are used as a reference for a model describing the effects produced by all the heavy constituents of cosmic rays with $Z \geq 6$, which appear to be highly efficient at inducing chemical reaction in ices. Considering the destruction cross-section values obtained by using eight different acetone bands, the average value of $3.5 \times 10^{-13} \text{ cm}^2$ is determined for pure acetone ice.

The formation and destruction cross-sections of the most abundant species formed in the ice (CH_4 , CO, H_2CO , CO_2 , C_2H_4 and C_2H_6) during the ion bombardment are determined to be in the range of 10^{-14} to 10^{-15} cm^2 , and for the molecular dissociation and chemical reactions around 10^{-14} .

Several authors have suggested that the destruction cross-section σ_d , because of fast ions, follows a power law as a function of the electronic stopping power S_e , and is $\sigma_d \sim S_e^n$, where $n \sim 1.3$ for the C–H destruction cross-section (Godard et al. 2011) and $n \sim 1.5$ (de Barros et al. 2011a, de Barros et al. 2014; Andrade et al. 2013), based on experiments with methanol, formic acid and a mixture of methanol + water ice. However, this n -value is not yet established and five n -values are considered here ($1 \leq n \leq 2$). Assuming the law $\sigma_d = aS_e^n$ with $n = 1.5$, the half-lives of acetone in the ISM close to the proximity of the Solar system and in the direction of the Galactic Centre due to the main ions (H, He, C, Mg, O, Si, Fe, Ni) are predicted to be 570 and 56.5 Ma, respectively. If $n = 1.0$ is considered, the interaction of hydrogen and helium ions with ice determines the acetone half-life, while if $1.25 \leq n \leq 2$, the acetone is mainly destroyed by heavier ions.

In addition, the penetration depths of some light and heavy ions in pure acetone ice are calculated. The results show that for velocities corresponding to $10^{-2} \leq E \text{ (MeV u}^{-1}) \leq 10^{-1}$, Fe and other heavy ions reach deeper layers than protons or He ions. In this way, Fe and other heavy ions rule the chemical reactions in the bulk. In this relatively low velocity range, the energy rate transferred to the ice by the heavy ions is 10 times higher than that of the light ions. Because of the interaction between projectiles and carbon atoms of acetone is strong, heavy ions penetrate deeper in the ice than H or He ions. For velocities close to the maximum cosmic ray flux in the ISM ($E/m = 50\text{--}100 \text{ MeV u}^{-1}$), heavy ions penetrate less than light ions, having a penetration depth about 10 times lower than hydrogen. Although heavy and light ions participate in inducing desorption, Fe and Ni ions transfer 10^3 times more energy than H and He ions when traversing $0.1 \text{ }\mu\text{m}$ of ice. C and O ions have approximately the same penetration depths as each other, which are intermediary values between those of Fe and H.

ACKNOWLEDGEMENTS

This work was supported by the French–Brazilian exchange programme CAPES-COFECUB. We are grateful to T. Been, C. Grygiel, T. Madi, I. Monnet, A. Domaracka, X.Y. Lv, T. Langlinay and J. M. Ramillon for their invaluable support. The Brazilian agencies CNPq (INEspaço) and FAPERJ are also acknowledged.

REFERENCES

- Almeida G. C., Pilling S., Andrade D. P. P., Castro N. L. S., Mendoza E., Boechat-Roberty H. M., Rocco M. L. M., 2014, *J. Phys. Chem. C*, 118, 6193
 Andrade D. P. P., de Barros A. L. F., Pilling S., Domaracka A., Rothard H., Boduch P., da Silveira E. F., 2013, *MNRAS*, 430, 787
 Bennett C. J., Jamieson C. S., Osamura Y., Kaiser R. I., 2006, *ApJ*, 653, 792

- Bennett C. J., Chen S. H., Un B. J., Chang A. H. H., Kaiser R. I., 2007, *ApJ*, 660, 1588
- Boogert A. C. A., Hogerheijde M. R., Blanke G. A., 2002, *ApJ*, 568, 761
- Boogert A. C. A. et al., 2008, *ApJ*, 678, 985
- Caselli P., Walmsley C. M., 2001, in Montmerle T., André P., eds, *ASP Conf. Ser. Vol. 243, From Darkness to Light: Origin and Evolution of Young Stellar Clusters*. Astron. Soc. Pac., San Francisco, p. 67
- Ceccarelli C. et al., 2002, *A&A*, 383, 603
- Combes F., Gerin M., Wootten A., Wlodarczak G., Clausset F., Encrenaz P. J., 1987, *A&A*, 180, L13
- D'Hendecourt L. B., Allamandola L. J., Grim R. J. A., Greenberg J. M., 1986, *A&A*, 158, 119
- Dartois E., Schutte W., Geballe T. R., Demyk K., Ehrenfreund P., D'Hendecourt L., 1999, *A&A*, 342, L32
- de Barros A. L. F., Domaracka A., Andrade D. P. P., Boduch P., Rothard H., da Silveira E. F., 2011a, *MNRAS*, 418, 1363
- de Barros A. L. F., Bordalo V., Duarte E. S., da Silveira E. F., Domaracka A., Rothard H., Boduch P., 2011b, *A&A*, 531, A160
- de Barros A. L. F., da Silveira E. F., Rothard H., Langlinay T., Boduch P., 2014, *MNRAS*, 443, 2733
- Ehrenfreund P., Charnley S. B., 2000, *AR&AA*, 38, 427
- Ehrenfreund P., Boogert A. C. A., Gerakines P. A., Tielens A. G. G. M., van Dishoeck E. F., 1997, *A&A*, 328, 649
- Friedel D. N., Snyder L. E., Remijan A. J., Turner B. E., 2005, *ApJ*, 632, L95
- Gerakines P. A., Schutte W. A., Greenberg J. M., van Dishoeck E. F., 1995, *A&A*, 296, 810
- Gerakines P. A., Schutte W. A., Ehrenfreund P., 1996, *A&A*, 312, 289
- Godard M. et al., 2011, *A&A*, 529, A146
- Goicoechea J. R., Rodriguez-Fernandez N. J., Cernicharo J., 2004, *ApJ*, 600, 214
- Groner P., Albert S., Herbst E., De Lucia F. C., Lovas F. J., Brian J. D., John C. P., 2002, *ApJS*, 142, 145
- Harris W. C., Levin I. W., 1972, *J. Mol. Spectrosc.*, 43, 117
- Harrison J. J., Allen N. D. C., Bernath P. F., 2011, *J. Quant. Spectrosc. Radiat. Transfer*, 112, 53
- Hüttemeister S., Wilson T. L., Mauersberger R., Lemme C., Dahmen G., Henkel C., 1995, *A&A*, 294, 667
- Jamieson C. S., Mebel A. M., Kaiser R. I., 2006, *ApJS*, 163, 184
- Kuan Y.-J., Snyder L. E., 1996, *ApJ*, 470, 981
- Martín-Pintado J., de Vicente P., Fuente A., Planesas P., 1997, *ApJ*, 482, L45
- Mejía C. F., de Barros A. L. F., Bordalo V., da Silveira E. F., Boduch P., Domaracka A., Rothard H., 2013, *MNRAS*, 433, 2368
- Minh Y. C., Haikala L., Hjalmarsen A., Irvine W. M., 1998, *ApJ*, 498, 261
- Murakami H., Koyama K., Maeda Y., 2001, *ApJ*, 558, 687
- Oka T., Geballe T. R., Goto M., Usuda T., McCall B. J., 2005, *ApJ*, 632, 882
- Peng T.-C. et al., 2013, *A&A*, 554, A78
- Pontoppidan K. M., Dartois E., van Dishoeck E. F., Thi W.-F., d'Hendecourt L., 2003a, *A&A*, 404, L17
- Pontoppidan K. M. et al., 2003b, *A&A*, 408, 981
- Prasad S. S., Tarafdar S. P., 1983, *ApJ*, 267, 603
- Ruiterkamp R., Peeters Z., Moore M. H., Hudson R. L., Ehrenfreund P., 2005, *A&A*, 440, 391
- Seperuelo Duarte E., Boduch P., Rothard H., da Silveira E. F., 2009, *A&A*, 502, 599
- Seperuelo Duarte E., Domaracka A., Boduch P., Rothard H., Dartois E., da Silveira E. F., 2010, *A&A*, 512, A71
- Snyder L. E., Lovas F. J., Mehringer D. M., Miao N. Y., Kuan Y. J., Hollis J. M., Jewell P. R., 2002, *ApJ*, 578, 245
- Tielens A. G. G. M., Tokunaga A. T., Geballe T. R., Baas F., 1991, *ApJ*, 381, 181
- van Broekhuizen F. A., Groot I. M. N., Fraser H. J., van Dishoeck E. F., Schlemmer S., 2006, *A&A*, 451, 723
- van der Tak F., van Dishoeck E., 2000, *A&A*, 358, L79
- van der Tak F. F. S., Walmsley C. M., Herpin F., Ceccarelli C., 2006, *A&A*, 447, 1011
- Ziegler J. F., Ziegler M. D., Biersack J. P., 2010, *Nucl. Instrum. Meth. Phys. Res. B*, 268, 1818

This paper has been typeset from a \LaTeX file prepared by the author.